

Micro-ring resonator based all optical reversible logic gates and its applications

G. K. BHARTI, J. K. RAKSHIT*

Department of Electronics & Instrumentation Engineering, National Institute of Technology Agartala, Tripura, India

In this paper, the silicon micro-ring resonator (MRR) as nonlinear all-optical switch is described through two-photon absorption (TPA) effect. The all-optical scheme of reversible Peres-gate, Toffoli-gate, Fredkin-gate and TR gate using MRR are presented in this paper. Simulation results confirming described method are also presented in this paper. We identified a combination of feasible MRR radius and coupling coefficient through numerical simulation which allows analyzing the system performance of the scheme, as extinction-ratio (ER) and contrast-ratio (CR), confirms the feasibility of design. The proposed circuit may perform different arithmetic and logic operations in the reversible logic-based information-processing.

(Received May 17, 2018; accepted February 12, 2019)

Keywords: Micro-ring resonator, Optical logic, Reversible logic gate

1. Introduction

Reversible logic is of increasing importance to many future computer technologies as a promising computing model with extensive applications in nanotechnologies such as quantum computing, quantum dot cellular automata, optical computing, etc [1-2]. A logic circuit is reversible if the circuit can generate unique output vector from each input vector, and vice versa, that is, there is a one-to-one mapping between the input and output vectors [3]. The main objective of the design and synthesis of reversible logic is to minimize the number of garbage outputs and the quantum cost. Garbage outputs refer to the unutilized outputs that are not used as primary outputs and which cannot be used as inputs for new computation, and are only needed to maintain one-to-one mapping. Each Reversible gate has a cost associated with it called quantum cost. The quantum cost of a reversible gate is the number of 2×2 Reversible gates or quantum logic gates required in designing the circuit. Reversible logic can also help in realizing dissipation less computing [4]. The power dissipation in a circuit can be reduced by the use of Reversible logic. Landauer's [5] principle states that irreversible computations generates heat of $KT \ln 2$ for every bit of information lost, where K is Boltzmann's constant and T the absolute temperature at which the computation performed. Bennett [6] showed that if a computation is carried out in Reversible logic zero energy dissipation is possible, as the amount of energy dissipated in a system is directly related to the number of bits erased during computation. There are significant differences in the synthesis technique of reversible logic circuits from the combinational one in many ways as follows: (1) Fan out is not permitted, that is, each output will be used only once; (2) Feedback is not permitted, that is the output of a gate can't be use as its input; (3) Use minimum number of

garbage outputs; (4) Use minimum circuit level; and (5) Use minimum number of gates.

A set of reversible gates are needed to design reversible circuit. Several such gates are proposed over the past decades. Among them, Fredkin gate, Toffoli gate and Peres gate are most common [7-9]. Arithmetic circuits such as Adders, Subtractors, Multipliers and Dividers are the essential blocks of a Computing system [10-22]. Dedicated Adder/Subtractor circuits are required in a number of digital signal processing applications. Several designs for binary Adders and Subtractors are investigated based on Reversible logic. However, there is not much existing work on reversible logic gates and binary adders and subtractors in optical domain. For increasing transmission capacity, Photon being the ultimate unit of information with unmatched speed and with data package in a signal of zero mass. Recently, researchers have also implemented reversible logic gates such as Toffoli gate, Peres gate and Modified Fredkin gate using different schemes like semiconductor optical amplifier (SOA)-based Mach-Zehnder interferometer (MZI), terahertz optical asymmetric demultiplexer (TOAD), quantum dot cellular automata-based system and microring resonator in optical domain [23-31]. The major limitations of TOAD switches are the finite length of fiber loop. The second limitation is due to SOA with slow recovery of the optical medium which limits the time required before the device can switch another pulse.

In this paper, we have proposed and designed all optical reversible gates such as Peres gate, Toffoli gate, Fredkin gate and TR gate using silicon waveguide based optical micro-ring resonator. Ring resonators are of particular interest for the design of optical components and systems, because of their ability to transmit very specific wavelength of light. It is also possible to fabricate compact micro-ring resonators with small radius, very high quality factor and reduced switching threshold which can lead to

high device integration densities and ultra-high speed for designing all optical circuits. We have also investigated the design of different arithmetic (half adder/subtractor, full adder and subtractor) circuits using micro-ring resonator in all optical reversible system. The performances of the proposed designs are better in terms of number of gates, garbage inputs/outputs and optical cost.

The paper is organized as follows: Section-1 presents a brief introduction to recent trend in reversible logic gates and optical information processing. In Section 2 principle and operation of silicon waveguide ring-resonator based optical switch is discussed. All-optical circuit for ring resonator based Peres gate, Toffoli gate, Fredkin gate and TR gate is reported in Section 3. Results and discussion are given in Section 4. Some applications of reversible logic gates are mentioned in Section 5. Finally Section 6 concludes the paper.

2. Micro-ring resonator and its application to design reversible logic gates

2.1. Principle operation of micro-ring resonator

The basic configuration of optical micro-ring-resonator (OMRR) consisting of unidirectional couplers with coupling coefficients κ_1 and κ_2 between a ring cavity and input-output bus waveguides is shown in Fig. 1(a). Optical micro-ring resonator can act as optical reservoir to accumulate the power only at a particular wavelength due to constructive interference. A constructive interference will take place when the optical path-length of a round trip is integer multiple of the effective wavelength and the OMRR will be 'ON' resonance. At 'ON' resonant, OMRR transmit the input port signal through the drop port and hence drop port shows high transmission and through port shows low transmission. If the OMRR is made up of nonlinear material, then the refractive index of OMRR depends on high intensity optical signal. The "ON" resonance condition can change its state temporarily by pumping high intensity optical pulse to the ring. Pumping induces the free carriers in the waveguide which change the refractive index of the material. The effective refractive index can be expressed as follows: $n_{\text{eff}} = n_0 + n_2$.

$I = n_0 + \frac{n_2}{S} \cdot P$, where n_0 and n_2 are the linear and non-linear refractive indexes of the material respectively. I and P are the intensity and power of the optical pump signal. S is the effective cross section area of the ring. The change of the refractive index of the micro-ring causes a temporarily shift of the micro-ring resonance wavelength. Practically an actively mode locked ring laser can be used to generate these pump pulses [32]. So when the pump pulse is applied to the ring, the resonance wavelength of OMRR will be shifted due to the change in refractive index, which shows high transmission at the through-port and low transmission at the drop-port. Again, when the pump pulse is released, the resonance wavelength shifts back to its original position producing high transmittance at the drop-port of the ring [33]. The through port and drop port output

electric fields is written by eq.(1) and eq.(2) respectively [33].

In order to determine the working wavelengths of MRR, the static response spectra (insertion loss) of the device at drop port and through port for two different conditions (pump on and pump off) is shown in Fig. 1(b). When no pump pulses applied to the ring, MRR will direct the input light to the drop port with minimum insertion loss of -0.965 dB and through port shows minimum transmission with high insertion loss of -32.9 dB at working wavelength of 1551.00 nm. With the pump pulses of 1.82 mW applied to MRR, MRR will direct the input light to the through port of the device with minimum insertion loss of -2.65 dB and drop port shows minimum transmission with high insertion loss of 31.3 dB at working wavelength of 1551.00 nm. Accordingly, the working wavelength of MRR is chosen at 1551.00 nm for switching operation. The operation of OMRR as all optical switches under pump – probe configuration is shown in Table 1. A high value of on-off ratio of around 31.9 dB is calculated from Fig. 1(b). Free spectral range (FSR) of 36 nm is also obtained from Fig. 1 (b).

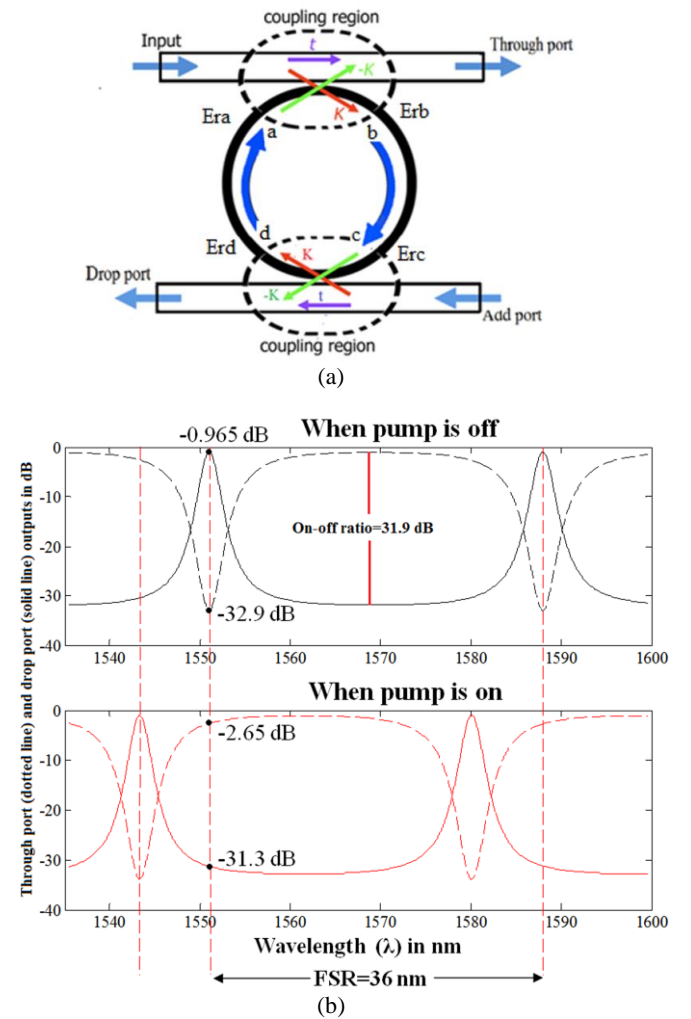


Fig. 1. (a): Single micro-ring resonator, (b): Insertion loss of the device at the output ports: Through port (dotted line) and drop port (solid line) outputs

Table 1. Truth table for OMRR-based switch

Input signal	Control (pump) signal	Drop-port output	Through-port output
0	0	0	0
0	1	0	0
1	0	1	0
1	1	0	1

Now we calculate phase shift and refractive index change due to application of pump pulse. We consider the case under pumping of ring by a pulsed laser, which induces TPA in the silicon material. This makes changes in the free carrier concentration including a change of electron concentration ΔN_e and a change of hole concentration (ΔN_h).

$$E_t = \frac{\sqrt{1-\kappa_1} - \sqrt{1-\kappa_2} \exp(-\alpha L) \exp^2(j\phi)}{1 - \sqrt{1-\kappa_1} \sqrt{1-\kappa_2} \exp(-\alpha L) \exp^2(j\phi)} E_{i1} + \frac{-\sqrt{\kappa_1} \sqrt{\kappa_2} \exp(-\alpha \frac{L}{2}) \exp(j\phi)}{1 - \sqrt{1-\kappa_1} \sqrt{1-\kappa_2} \exp(-\alpha L) \exp^2(j\phi)} E_{i2} \quad (1)$$

$$E_d = \frac{-\sqrt{\kappa_1} \sqrt{\kappa_2} \exp(-\alpha \frac{L}{2}) \exp(j\phi)}{1 - \sqrt{1-\kappa_1} \sqrt{1-\kappa_2} \exp(-\alpha L) \exp^2(j\phi)} E_{i1} + \frac{\sqrt{1-\kappa_2} - \sqrt{1-\kappa_1} \exp(-\alpha L) \exp^2(j\phi)}{1 - \sqrt{1-\kappa_1} \sqrt{1-\kappa_2} \exp(-\alpha L) \exp^2(j\phi)} E_{i2} \quad (2)$$

where, $\kappa_n = \frac{2\pi}{\lambda} n_{eff}$, is wave propagation constant,

$\phi = \frac{\kappa_n \cdot L}{2}$, L is length of the ring, E_{i1} and E_{i2} are the input and add port fields respectively.

The non-linear refractive-index change at wavelength of 1.55 μm is given by [34-35]

$$\Delta n = \Delta n_e + \Delta n_h = - \left[8.8 \times 10^{-22} \Delta N + 8.5 \times 10^{-22} (\Delta N)^{0.8} \right] \quad (3)$$

where, $\Delta N = \Delta N_e = \Delta N_h$

The negative sign in eq.(3) shows that effectively result in a net decrease of the refractive index of the micro-ring waveguide and cause a temporarily blue shift of the micro-ring resonance wavelength.

The free-carrier concentration N in the silicon waveguide is generated by TPA, so its rate of generation is given by [36]:

$$\frac{dN}{dt} = \frac{\beta I^2}{2h\nu} \quad (4)$$

where I is the light intensity, $h\nu$ is the photon energy and β is the TPA coefficient.

The phase shift change of the signal light at 1.55 μm in one circle of the ring is given by

$$\phi = \frac{2\pi}{\lambda} \Delta n L \quad (5)$$

Refractive-index change,

$$\Delta n = - \left[8.8 \times 10^{-22} \frac{\beta t_p^2}{2h\nu \sqrt{\pi} \tau S^2} P_{avg}^2 + 8.5 \times 10^{-22} \left(\frac{\beta t_p^2}{2h\nu \sqrt{\pi} \tau S^2} P_{avg}^2 \right)^{0.8} \right] \quad (6)$$

where, P_{avg} is the average pump power with pulse separation t_p and pulse width τ and L is length of the ring.

The curve of phase shift can be obtained from eq.(5) using the following data [36]: $\beta = 7.9 \times 10^{-10}$ cm/W, pump beam wavelength, $\lambda_p = 400$ nm, $\tau = 100$ fs, $t_p = 12.5$ ns, $h\nu = 49.725 \times 10^{-20}$ J, radius of the ring, $r = 3.05$ μm , $S = 450 \times 250$ nm², $n_2 = 4 \times 10^{-18}$ m²/W, coupling coefficient, $K_s = 0.22$. The practical realization of such coupling coefficient is difficult because the coupling coefficient cannot be determined with the high accuracy. One possible solution would be to use tunable couplers. The graph for phase shift with average pump power is shown in Fig. 2. It can be shown from Fig. 2 that when the phase shift approaches π , the average pump power required for switching is only 1.82 mW. We found from Fig. 1(b) on-off ratio 14.95 dB and free spectral range (FSR) of 16 nm. A small phase shift can result in an enough extinction ratio but amplitude modulation (AM) would be very high. For complete switching phase shift should be π [35].

The Kerr effect causes a very small red-shift of the resonance. However, the changes in refractive index due to TPA effect result in a linear shift of the complex resonance frequency of the cavity which is much much higher than that Kerr effect, so the blue shift dominates. Also in [37], it is shown that switching power of Kerr-type ring switches is about 3 orders larger than that of TPA-type ring switches. The reason for this is that the nonlinear phase shift caused by the Kerr effect is proportional to the self-pumping power. Whereas, the nonlinear phase shift caused by the TPA effect is appreciatively proportional to the square of average pump power (see Fig. 2).

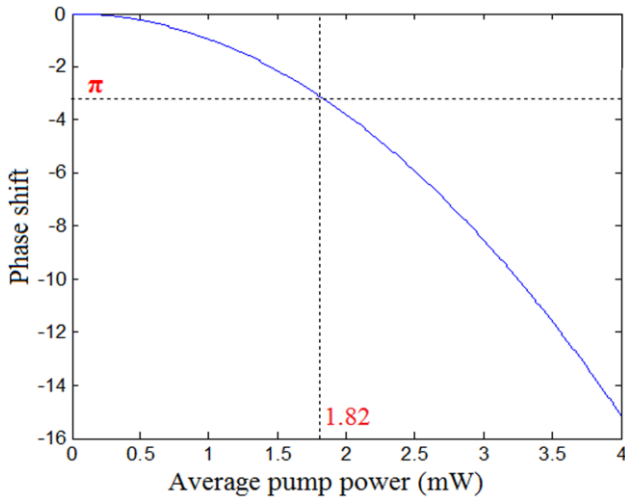


Fig. 2. Phase shift in the ring resonator as a function of average pump power

2.2. Theoretical model for all optical reversible logic gates using micro-ring resonator

2.2.1. Ring resonator based Peres gate

The Peres gate is a 3-input 3-output (3×3) reversible gate having the three inputs (A, B, C) and three outputs (X, Y, Z) satisfy the relationship as follows:

$$X = A, \quad (7a)$$

$$Y = A \oplus B, \quad (7b)$$

$$Z = A.B \oplus C \quad (\text{where "A.B" stands for 'A' AND 'B'}) \quad (7c)$$

Fig. 3(a) shows the block diagram of Peres gate and Table 2 shows its corresponding truth table.

The ring resonator based circuit for all-optical reversible Peres gate is given in Fig. 3(b). MRR1 and MRR2 will perform the XOR operation as discussed in previous section. The operational principle of this gate is discussed below in details.

Case-1: ($A = C = 0$ and $B = 1$)

The input signal applied to input port of MRR3 will be directed to its drop port as the control signal 'A' is at low level and act as input signal of MRR5. As pump pulse 'C' at MRR5 is at low level, the input signal will be directed to its drop port and the through port of MRR5 produces output 'Z'=0. Therefore, when $A = C = 0$ and $B = 1$, then the final outputs $X = 0$, $Y = 1$, $Z = 0$ which satisfies the third row of the truth Table 2.

Case-2: ($A = 1$, $B = 0$ and $C = 1$)

The input signal applied to input port of MRR3 will be directed to its through port as the control signal 'A' is at high level and act as input signal of MRR4. As control

pulse 'B' is at low level, the input signal to MRR4 will be directed to its drop port which act as input for MRR5. As pump pulse 'C' at MRR5 is at high level, the input signal will be directed to its through port and produces final output $Z=1$.

Hence, the final outputs are $X = 1$, $Y = 1$ and $Z = 1$ which satisfies the sixth row of the truth Table 2. Similarly the other cases can be explained following the truth Table 2.

Table 2. Truth table of Peres gate

Inputs			Outputs		
A	B	C	X	Y	Z
0	0	0	0	0	0
0	0	1	0	0	1
0	1	0	0	1	0
0	1	1	0	1	1
1	0	0	1	1	0
1	0	1	1	1	1
1	1	0	1	0	1
1	1	1	1	0	0

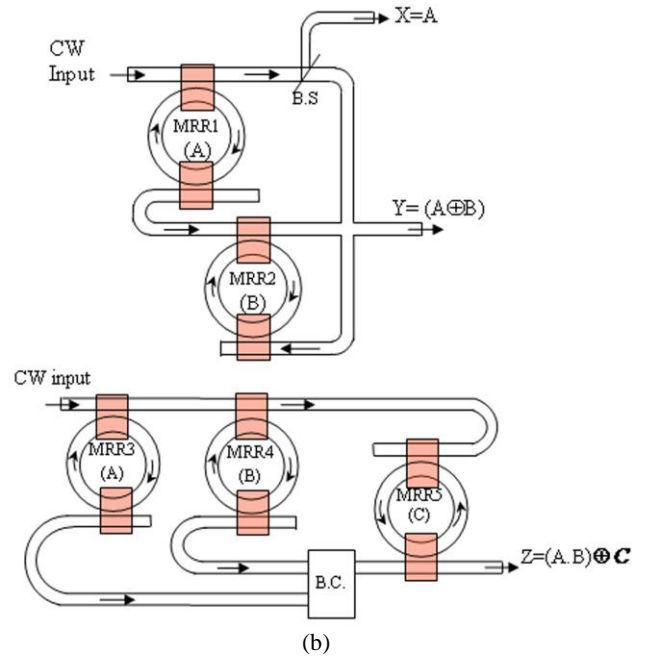
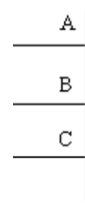


Fig. 3. (a) Block diagram of Peres gate, (b): All-optical Peres gate (PG). MRR: Micro-ring resonator, B.S: beam Splitter, B.C: Beam Combiner, A: Input A, B: Input B, C: Input C

2.2.2. Ring resonator based Toffoli gate

The Toffoli Gate (TG) is a 3×3 two-through reversible gate. Two-through means two of its outputs are the same as the inputs. It has three inputs (A, B, C) and three outputs (X, Y, Z) satisfy the relationship as follows:

$$X = A, \quad (8a)$$

$$Y = B, \quad (8b)$$

$$Z = A.B \oplus C \quad (8c)$$

Fig. 4(a) shows the block diagram of Toffoli gate and Table 3 shows its corresponding truth table.

Table 3. Truth table of Toffoli gate

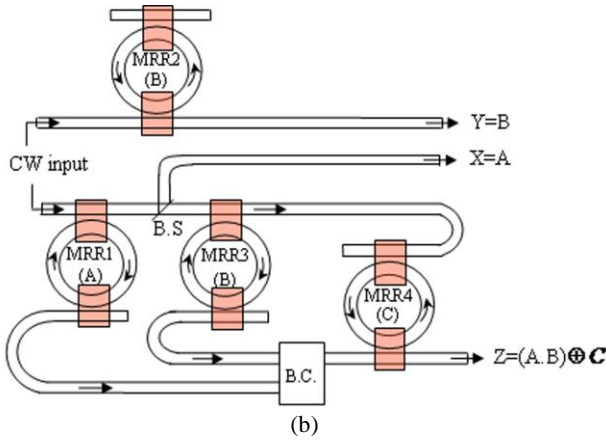
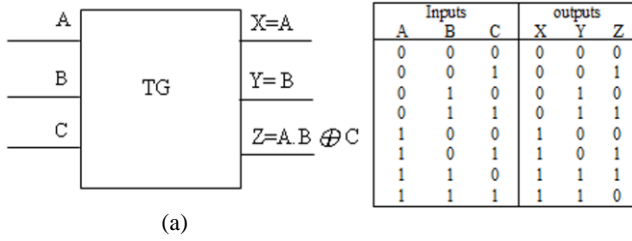


Fig. 4. (a) Block diagram of Toffoli gate (b): All-optical Toffoli gate (TG). MRR: Micro-ring resonator, B.S: beam Splitter, B.C: Beam Combiner, A: Input A, B: Input B, C: Input C

The ring resonator based circuit for all-optical reversible Toffoli gate is given in Fig. 4(b). Here continuous wave (CW) is applied to the input ports of MRR1 and MRR2. The operational principle of this gate is discussed below in details.

Case-1: ($A = C = 0$ and $B = 1$)

The incoming signal at the input port of MRR2 will be directed to its through port as pump pulse 'B' applied to MRR2 is at high level which produces output $Y=1$. The incoming signal at the input port of MRR-1 will be directed to its drop port as pump pulse 'A' applied to MRR-1 is at low level which shows output $X=0$. The drop port output of MRR-1 acts as input of MRR4 and that signal will be directed to its drop port and through port will detect no light ($Z=0$) as pump pulse 'C' applied to MRR4 is at low level. Therefore, when $A = C = 0$ and $B = 1$ then $X = 0$, $Y = 1$ and $Z = 0$. It satisfies the third row of the truth Table 3.

Case-2: ($A = 1$ and $B = C = 0$)

The incoming signal at the input port of MRR-2 will be directed to its drop port as pump pulse 'B' applied to

MRR2 is at low level which produces output $Y=0$. The incoming signal at the input port of MRR-1 will be directed to its through port as pump pulse 'A' applied to MRR-1 is at high level which shows output $X=1$. The through port output of MRR-1 acts as input of MRR3 and that signal will be directed to its drop port as pump pulse 'B' is at low level. The drop port output of MRR3 acts as input of MRR4 and that signal will be directed to its drop port and through port will detect no light ($Z=0$) as pump pulse 'C' applied to MRR4 is at low level. Therefore, when $A = C = 0$ and $B = 1$ then $X = 0$, $Y = 1$ and $Z = 0$. It satisfies the third row of the truth Table 3. Hence, the final outputs are $X = 1$, $Y = Z = 0$ When $A = 1$ and $B = C = 0$. It satisfies the fifth row of the truth Table 3. Similarly the other cases can be explained following the truth Table 3.

2.2.3. Ring resonator based Fredkin gate

The Fredkin Gate (FG) is a 3×3 reversible gate. It has three inputs (A, B, C) and three outputs (X, Y, Z) satisfy the relationship as follows:

$$X=A, \quad (9a)$$

$$Y=\overline{AB} + AC \quad (9b)$$

$$Z= AB + \overline{AC} \quad (9c)$$

Fig. 5(a) shows the block diagram of Fredkin gate and Table 4 shows its corresponding truth table.

Table 4. Truth table of Fredkin gate

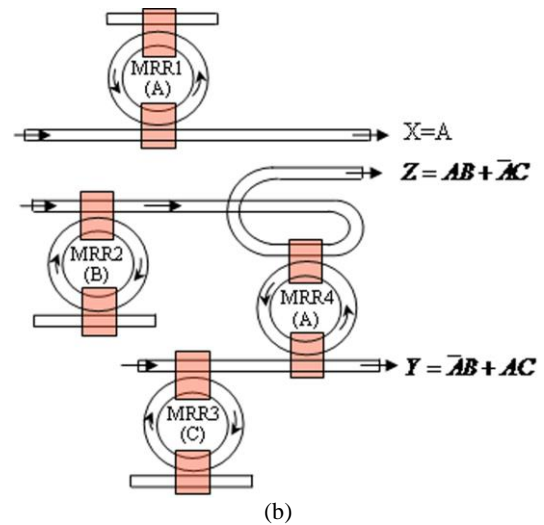
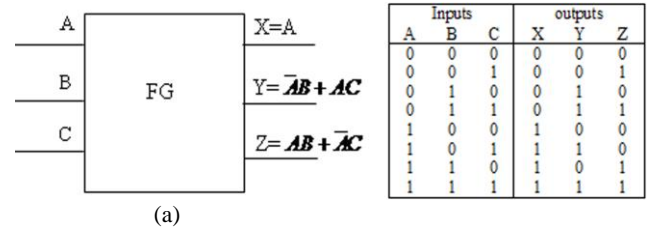


Fig. 5. (a) Block diagram of Fredkin gate (b): All-optical circuit of Fredkin gate (FG). A: Input A, B: Input B, C: Input C

The ring resonator based circuit for all-optical reversible Fredkin gate is given in Fig. 5(b). Here input signal is applied to the input ports of MRR1, MRR2 and MRR3. The operational principle of this gate is discussed below in details.

Case-1: ($A = C = 0$ and $B = 1$)

The incoming optical signal applied to the input port of MRR1 will be directed to its drop port and produce output $X=0$ at its through port as control pulse 'A' is absent. At the same time the incoming optical signal is also applied to MRR2 and MRR3 simultaneously and as control signal 'B' is at high level the input optical signal will be directed to the through port MRR2 which will again directed to the through port of MRR4 produces the final output 'Y'=1 as control signal 'A' is at low level. The input optical signal which is applied to the input port of MRR3 will be directed to its drop port and no signal will be directed to the input of MRR4 which produces the final output 'Z'=0 as control pulse 'C' is at low level. Therefore, when $A = C = 0$ and $B = 1$ then $X = 0$, $Y = 1$ and $Z = 0$ and it satisfies the third row of the truth Table 4.

Case-2: ($A = 1$, $B = 0$ and $C = 1$)

The incoming optical signal applied to the input port of MRR1 will be directed to its through port and produce final output $X=1$ at its through port as control pulse 'A' is present. At the same time the incoming optical signal is also applied to MRR2 and MRR3 simultaneously and as control signal 'B' is at low level the input optical signal will be directed to the drop port MRR2. The input optical signal which is applied to the input port of MRR3 will be directed to its through port which will again directed to the through port of MRR4 produces the final output 'Y'=1 and 'Z'=0 as control signal 'A' is at high level. Hence, the final output is $X = 1$, $Y = 1$ and $Z = 0$ which satisfies the sixth row of the truth Table 4. Similarly the other cases can be explained following the truth Table 4.

2.2.4. Ring resonator based TR gate

The TR Gate is a 3×3 reversible gate. It has three inputs (A, B, C) and three outputs (X, Y, Z) satisfy the relationship as follows:

$$X = A, \quad (10a)$$

$$Y = A \oplus B \quad (10b)$$

$$Z = A \cdot \bar{B} \oplus C \quad (10c)$$

Fig. 6(a) shows the block diagram of TR gate and Table 5 shows its corresponding truth table.

Table 5. Truth table of TR gate

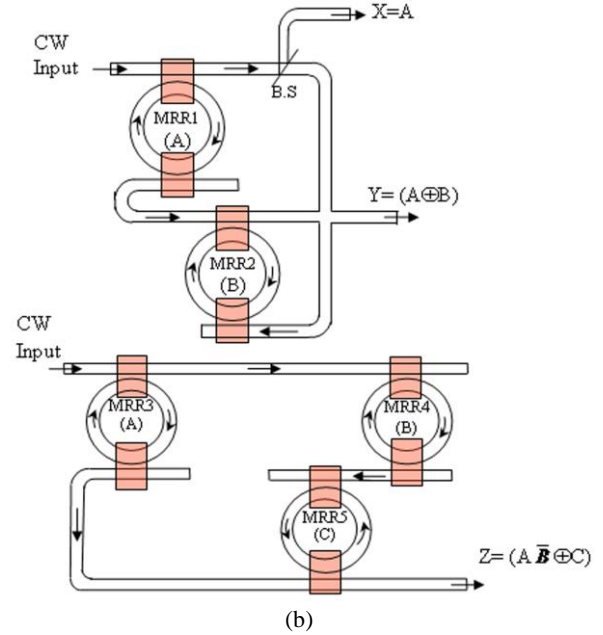
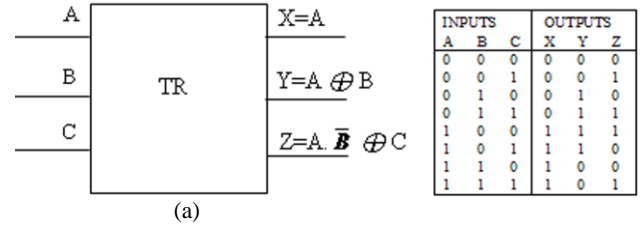


Fig. 6. (a) Block diagram of TR gate, (b): All-optical circuit of TR gate. MRR: Micro-ring resonator, B.S: beam splitter, A: Input A, B: Input B, C: Input C

The ring resonator based all-optical reversible TR gate is given in Fig. 6(b). MRR1 and MRR2 will perform the XOR operation as discussed in previous section. The operational principle of this gate is discussed below in details.

Case-1: ($A = C = 0$ and $B = 1$)

The incoming optical signal which is applied to the input port of MRR3 will be directed to its drop port as the control signal 'A' is at low level. The drop port output of MRR3 act as input signal of MRR5 and will be directed to its drop port as the control signal 'C' is at low level. No signal will be detected at the through port which produces no final output at 'Z'=0. Therefore, when $A = C = 0$ and $B = 1$ then $X = 0$, $Y = 1$ and $Z = 0$. It satisfies the third row of the truth Table 5.

Case-2: ($A = 1$, $B = 0$ and $C = 1$)

The incoming optical signal which is applied to the input port of MRR3 will be directed to its through port as the control signal 'A' is at high level. The through port output of MRR3 act as input signal of MRR4 and will be

directed to its drop port which again directed to drop port of MRR5 as the control signals 'B' and 'C' are at low and high level respectively. No signal will be detected at the through port of MRR5 which produces no final output at 'Z'=0. Hence, the final output is $X = 1$, $Y = 1$ and $Z = 0$ which satisfies the sixth row of the truth Table 5. Similarly the other cases can be explained following the truth Table 5.

3. Results

Silicon waveguide based micro-ring resonator is a powerful device to realize the ultra-fast all optical switch. The advantage of silicon waveguide based MRR is that the overall losses can be relatively low [38]. Pure silicon has an absorption loss much smaller than 0.1 dB/cm at a wavelength of 1.55 μm . Scattering loss is also very low. Curvature loss is in negligible levels. Insertion loss is also very low at the wavelength of 1.55 μm .

We have conducted numerical simulations to validate the proposed model and analyze the reversible logic circuit performance for non-return-to-zero (NRZ) input data pulse format using MATLAB simulation platform. The transmission eq. (1) and eq. (2) is utilized to obtain the simulation results. The simulation work of all optical reversible logic gates is carried out on silicon waveguide based micro-ring resonator. Silicon waveguide based micro-ring resonator is a powerful device to realize the ultra-fast all optical switch. We choose probe input beam power 0.1mW such that there is no variation of refractive index of the material of OMRRs for input probe beam and other parameters as mentioned in the section 2. The proposed model can also handle pulses of return-to-zero (RZ) data format, which are widely used in modern optical communications, and can be generated by appropriate laser sources [39]. Data rate of the circuit for simulation is considered as 100 Gbps and maximum speed can be extended up to 250 Gbps [40-41].

Fig. 7(a) shows the simulation result for Peres gate where inputs $A = [0\ 0\ 0\ 0\ 1\ 1\ 1\ 1]$, $B = [0\ 0\ 1\ 1\ 0\ 0\ 1\ 1]$ and $C = [0\ 1\ 0\ 1\ 0\ 1\ 0\ 1]$ with the corresponding outputs $X = [0\ 0\ 0\ 0\ 1\ 1\ 1\ 1]$, $Y = [0\ 0\ 1\ 1\ 1\ 1\ 0\ 0]$ and $Z = [0\ 1\ 0\ 1\ 0\ 1\ 1\ 0]$.

Fig. 7(b) shows the simulation result for Toffoli gate where inputs $A = [0\ 0\ 0\ 0\ 1\ 1\ 1\ 1]$, $B = [0\ 0\ 1\ 1\ 0\ 0\ 1\ 1]$ and $C = [0\ 1\ 0\ 1\ 0\ 1\ 0\ 1]$ with the corresponding outputs $X = [0\ 0\ 0\ 0\ 1\ 1\ 1\ 1]$, $Y = [0\ 0\ 1\ 1\ 0\ 0\ 1\ 1]$ and $Z = [0\ 1\ 0\ 1\ 0\ 1\ 1\ 0]$.

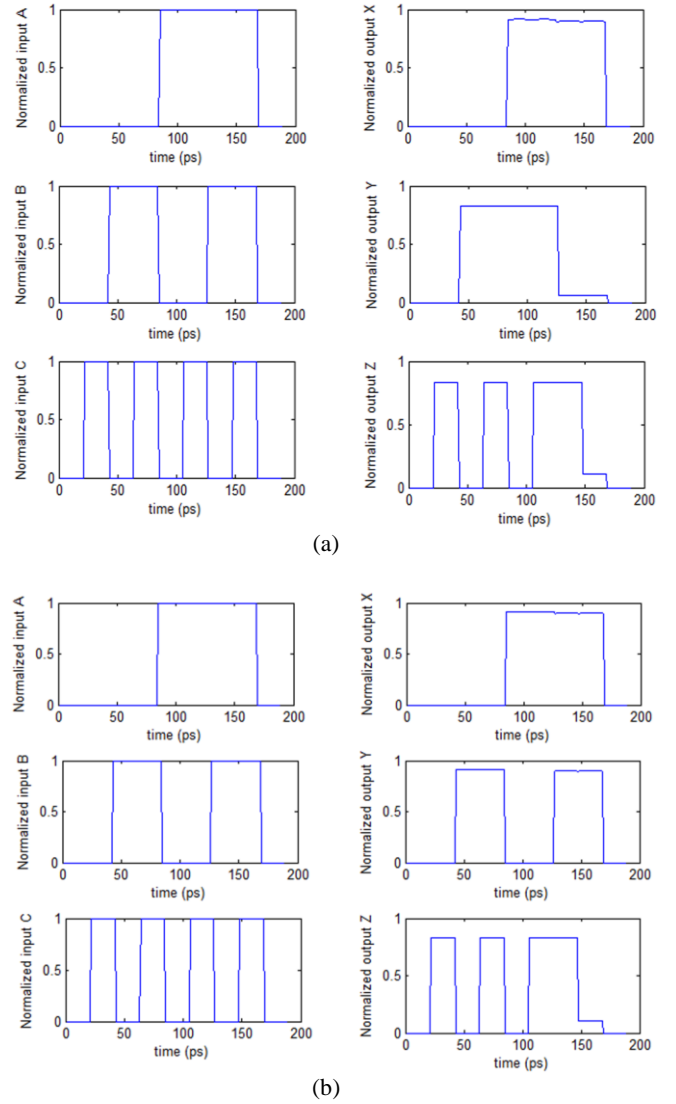


Fig. 7. (a) Simulation result for Peres gate, (b): simulation result for Toffoli gate

Fig. 8(a) shows the simulation result for Fredkin gate where inputs $A = [0\ 0\ 0\ 0\ 1\ 1\ 1\ 1]$, $B = [0\ 0\ 1\ 1\ 0\ 0\ 1\ 1]$ and $C = [0\ 1\ 0\ 1\ 0\ 1\ 0\ 1]$ with the corresponding outputs $X = [0\ 0\ 0\ 0\ 1\ 1\ 1\ 1]$, $Y = [0\ 0\ 1\ 1\ 0\ 1\ 0\ 1]$ and $Z = [0\ 1\ 0\ 1\ 0\ 0\ 1\ 1]$.

Fig. 8(b) shows the simulation result for TR gate where inputs $A = [0\ 0\ 0\ 0\ 1\ 1\ 1\ 1]$, $B = [0\ 0\ 1\ 1\ 0\ 0\ 1\ 1]$ and $C = [0\ 1\ 0\ 1\ 0\ 1\ 0\ 1]$ with the corresponding outputs $X = [0\ 0\ 0\ 0\ 1\ 1\ 1\ 1]$, $Y = [0\ 0\ 1\ 1\ 1\ 1\ 0\ 0]$ and $Z = [0\ 1\ 0\ 1\ 1\ 0\ 0\ 1]$.

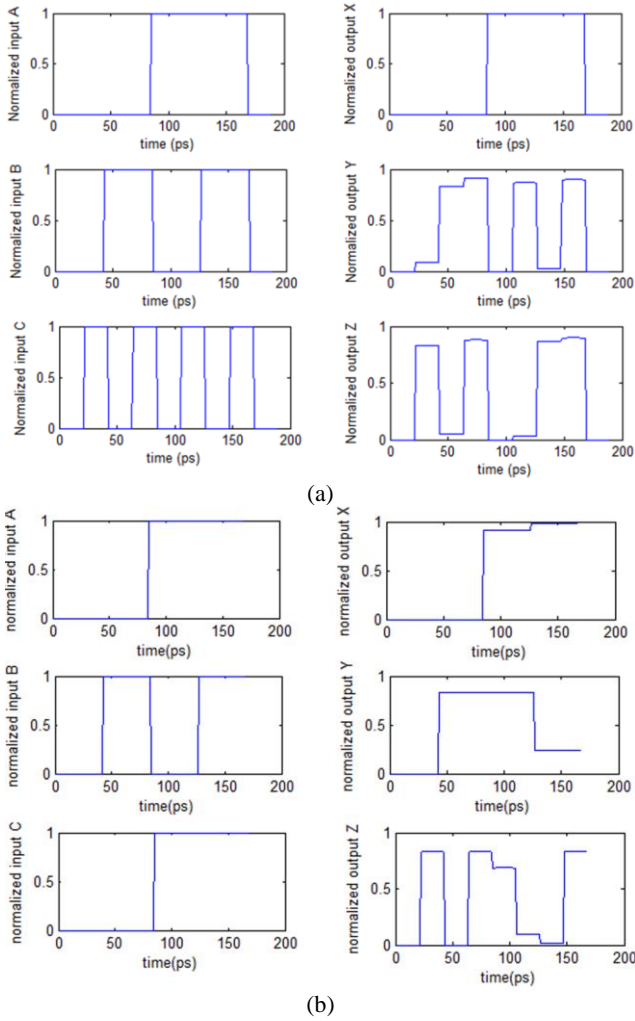


Fig. 8. (a) Simulation result for Fredkin gate, (b): Simulation result for TR gate

In order to evaluate the performance of the gates, we define and calculate different metrics such as optical delay, optical cost, garbage output, extinction ratio (ER), contrast ratio (CR) [42-43]. The optical cost of an all optical reversible logic gate is the number of optical switches required to design the reversible logic gate. Further, delay constitutes an important metric, the delay of each 1×1 gate and 2×2 reversible gate is taken as unit delay called Δ . Another most important features of a reversible gate is its garbage output i.e., every output of the gate which is not used as input to other gate or as a primary output is called garbage output.

As the Toffoli gate [Fig. 4(b)] and Fredkin gate [Fig. 5(b)] can be implemented using 4 ring resonator based optical switches thus the optical cost of Toffoli gate and Fredkin gate is same and is considered as 4. As the Peres gate [Fig. 3(b)] and TR gate [Fig. 6(b)] can be implemented using 5 ring resonator based optical switches thus the optical cost of Fredkin gate is considered as 5.

The high value of extinction ratio (ER) distinguishes between the high ('1') levels to the low ('0') levels very clearly. The ER can be defined as

$$ER \text{ (dB)} = 10 \log \left(\frac{P_{\min}^1}{P_{\max}^0} \right) \quad (11)$$

where P_{\min}^1 and P_{\max}^0 are the minimum and maximum values of the peak intensity of high ('1') and low ('0') level respectively. We have plotted ER against the different coupling coefficient with constant radius (3.05 μm) of the ring for the above seven reversible logic gates and are shown in Fig. 9(a). Similarly we have also plotted ER against the different radius with constant coupling coefficient (0.22) for the above seven reversible logic gates and are shown in Fig. 9(b). From Fig. 9(a,b), the maximum value of ER is obtained as 12.23 dB for Fredkin reversible logic gate at the optimum operating point.

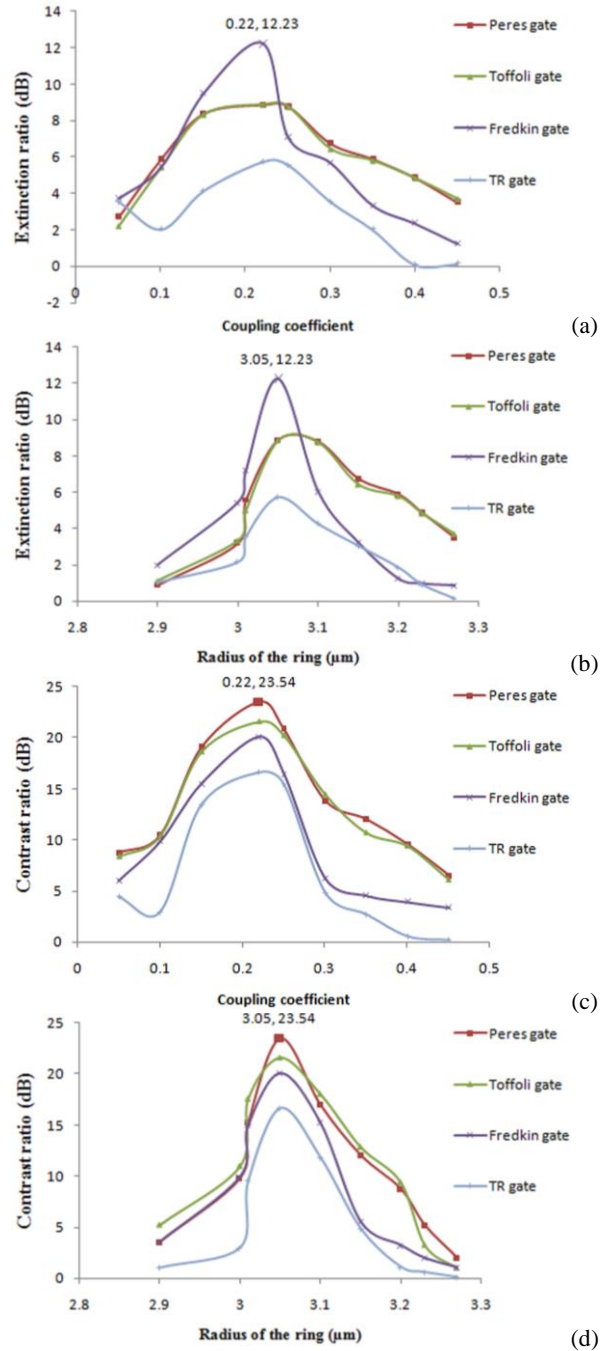


Fig. 9. (a) Extinction ratio against coupling coefficient, (b) extinction ratio against radius of the ring, (c) contrast ratio against coupling coefficient, (d) contrast ratio against radius of the ring

The eq. (1) and eq. (2) and the output simulation results of Fig. 7 and Fig. 8 are employed to obtain different values of ER and CR at various values for coupling coefficients as well as for the radius of the MRR respectively.

The output contrast ratio (CR) is defined as the ratio of mean value of output intensity for '1' (P_{mean}^1) to the mean output intensity for '0' (P_{mean}^0) and given as

$$CR \text{ (dB)} = 10 \log \left(\frac{P_{mean}^1}{P_{mean}^0} \right) \quad (12)$$

We have plotted CR against the different coupling coefficient with constant radius (3.05 μm) of the ring for the above seven reversible logic gates and are shown in Fig. 9(c). Similarly we have also plotted CR against the different radius with constant coupling (0.22) coefficient for the above seven reversible logic gates and are shown in Fig. 9(d). From Fig. 9(c,d), the maximum value of CR is obtaining as 23.54 dB for Peres reversible logic gate at the optimum operating point.

4. Discussion and applications of reversible logic gates

4.1. Reversible half adder/subtractor composite circuit

The all optical reversible half Adder/Subtractor Design consists of one Toffoli gate (TG) and one TR gate and their interconnections are shown in the Fig. 10. The numbers of Garbage inputs are 2 represented by logical zero and the Garbage output is only 1 represented by G. The proposed design of all optical reversible half adder/subtractor is optimized in terms of the optical cost, the delay and garbage output compared to the existing counterparts [44].

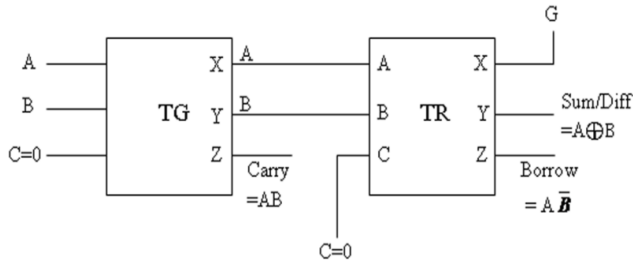


Fig. 10. Circuit for all optical reversible half Adder/Subtractor

4.2. Reversible full adder and subtractor circuit

The all optical reversible full Adder Design consists of two PG gates only, and their interconnections are shown in the Fig. 11. The numbers of garbage inputs are 2

represented by logical zero. The Garbage outputs are 2 represented by G1 to G2.

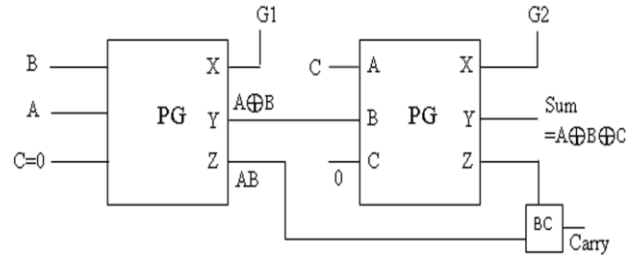


Fig. 11. Circuit for all optical reversible full Adder

The all optical reversible full Subtractor Design consists of two TR gates only, and their interconnections are shown in the Fig. 12. The numbers of garbage inputs are 1 represented by logical zero. The Garbage outputs are 2 represented by G1 to G2.

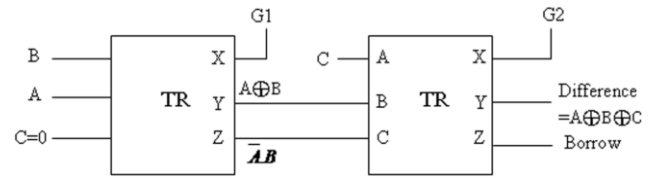


Fig. 12. Circuit for all optical reversible full subtractor

5. Conclusion

In this paper, the possibility of using silicon waveguide based MRRs as nonlinear all-optical switches is described through TPA effect. Silicon waveguide based MRRs allow lower propagation losses and lower fabrication cost and required low pump power of 1.82 mW. The all-optical scheme of reversible Peres gate, Toffoli gate, Fredkin gate and TR gate using silicon waveguide based micro-ring resonator are presented and described in this paper. Simulation results confirming described method are also presented in this paper. The variation of extinction ratio (ER) and contrast ratio (CR) with coupling coefficient and radius of the ring are also studied and satisfactory results obtained. Different arithmetic (half adder/subtractor, full adder and subtractor) operations in reversible system are also designed with these gates. The proposed designs are optimized in terms of the optical cost and the delay and garbage output compared to the existing counterparts. The theoretical models developed and the simulation results obtained will be useful to perform different arithmetic and logic operations in the reversible logic-based optical information processing.

References

- [1] E. Fredkin, Physica D: Nonlinear Phenomena **45**(1), 254 (1990).

- [2] X. Song, G. Yang, M. Perkowski, Y. Wang, Theory of Computing Systems **39**(2), 311 (2006).
- [3] P. Gupta, A. Agrawal, N. K. Jha, IEEE Transactions on Computer-Aided Design of Integrated Circuits and Systems, **25**(11), 2317 (2006).
- [4] C. H. Bennett, D. P. DiVincenzo, Nature **404**, 247 (2000).
- [5] R. Landauer, IBM J. Research and Development **5**, 183 (1961).
- [6] C. H. Bennett, IBM J. Research and Development **17**, 525 (1973).
- [7] N. Kostinski, M. P. Fok, P. R. Prucnal, Opt. Lett. **34**(18), 2766 (2009).
- [8] D. Maslov, G. W. Dueck, Electronics Letters **39**(25), 1790 (2003).
- [9] A. Peres, Phys. Rev. A **32**, 3266 (1985).
- [10] G. Li, L. Liu, L. Shao, Y. Yin, J. Hua, Applied Optics **36**(5), 1011 (1997).
- [11] G. Li, F. Qian, H. Ruan, L. Liu, Applied Optics **38**(23), 5039 (1999).
- [12] M. Ramachandran, S. Prince, D. Verma, Journal of Computational Electronics **17**(2), 845 (2018).
- [13] G. Li, F. Qian, H. Ruan, L. Liu, Optical Engineering **38**(3), 403 (1999).
- [14] F. Qian, G. Li, H. Ruan, H. Jing, L. Liu, Applied Optics **38**(26), 5621 (1999).
- [15] J. K. Rakshit, J. N. Roy, Journal of Computational Electronics **15**(4), 1450 (2016).
- [16] F. Qian, G. Li, H. Ruan, L. Liu, Optics & Laser Technology **31**, 403 (1999).
- [17] G. Li, F. Qian, Optical Engineering **40**(11), 2446 (2001).
- [18] A. Kotb, K. E. Zoiros, C. Guo, Optics & Laser Technology **108**, 426 (2018).
- [19] G. Li, L. Liu, J. Hua, L. Shao, Optics & Laser Technology **29**(4), 221 (1997).
- [20] G. Li, L. Liu, L. Shao, Y. Yin, Applied Optics **34**(8), 1321 (1995).
- [21] J. K. Rakshit, J. N. Roy, Photonic Network Communications **34**(1), 84 (2017).
- [22] Q. Feng, G. Li, M. S. Alam, Optical Engineering **40**(2), 275 (2001).
- [23] G. K. Maity, J. N. Roy, S. P. Maity, Springer Berlin Heidelberg Communications in Computer and Information Science, book series **192**, 249 (2011).
- [24] C. Taraphdar, T. Chattopadhyay, J. N. Roy, Optics & Laser Technology **42**(2), 249 (2010).
- [25] T. Chattopadhyay, IEEE Journal of Selected Topics in Quantum Electronics **18**(2), 585 (2012).
- [26] S. Kotiyal, H. Thapliyal, N. Ranganathan, IEEE Computer Society Annual Symposium on VLSI, 207 (2012).
- [27] A. J. Poustite, K. J. Blow, Optics Communications **174**(1-4), 317 (2000).
- [28] T. Purkayastha, T. Chattopadhyay, D. De, Nanotechnology Reviews **4**(5), 375 (2015).
- [29] J. N. Roy, J. K. Rakshit, International Conference on Fibre Optics and Photonics, Optical Society of America, S4B-6 (2014).
- [30] T. Chattopadhyay, IEEE Journal of Quantum Electronics **51**(4), 1 (2015).
- [31] P. Sethi, S. Roy, Special Issue on Reversible Computing, Springer Transactions on Computational Science **XXIV**, LNCS 8911, 21 (2014).
- [32] K. E. Zoiros, T. Houbavlis, M. Moyssidis, Opt. Commun. **254**, 310 (2005).
- [33] J. K. Rakshit, T. Chattopadhyay, J. N. Roy, Optik-International Journal for Light and Electron Optics **124**(23), 6048 (2013).
- [34] V. R. Almeida, Q. Xu, M. Lipson, Optics Letters **30**(18), 2403 (2005).
- [35] C.-F. Li, Na. Dou, Chin. Phys. Lett. **26**(5) 054203 (2009).
- [36] J. K. Rakshit, J. N. Roy, Optica Applicata **46**(4), 517 (2016).
- [37] J. K. Rakshit, J. N. Roy, Journal of Computational Electronics **15**(4), 1450 (2016).
- [38] B. E. Little, et al., Photonics Technology Letters, IEEE **10**(4), 549 (1998).
- [39] K. Zoiros et al., Optics Communications **180**, 301 (2000).
- [40] J. K. Rakshit, J. N. Roy, Journal of Computational Electronics **15**(4), 1450 (2016).
- [41] G. K. Bharti, J. K. Rakshit, Photonic Network Communications **35**(3), 381 (2018).
- [42] J. K. Rakshit, J. N. Roy, T. Chattopadhyay, 5th International Conference on Computers and Devices for Communication (CODEC), IEEE, 1-4 (2012, December).
- [43] J. K. Rakshit, J. N. Roy, Optica Applicata **44**(1), 39 (2014).
- [44] H. G. Rangaraju, U. Venugopal, K. N. Muralidhara, K. B. Raja, International Journal of VLSI Design & Communication Systems **1.3**, 23 (2010).

*Corresponding author: jayantarakshit.eie@nita.ac.in